Journal Name

ARTICLE TYPE

Fiber optic cadmium ion sensor based on functionalization of magnetic ion-imprinted polymer

Tao Shen,[a,b] Tianyu Yang,[a] Yue Feng,*[b] Xin Liu,[a] Chi Liu,[a] Weixiang Yuan,[a], Haodong Wu[b], and Chao Wang[c]

Cadmium poisoning is a chronic accumulation process, and even long-term drinking of low cadmium content water will cause kidney damage, so ultra-low detection limit is particularly important. However, at the present stage, the traditional detection method cannot reach the lower detection limit, and the response time cost of detection is also very high, so that the real-time measurement cannot be realized. Therefore, the traditional cadmium ion detection method has a slow response and an insufficient detection limit. This paper presents a fiber optic cadmium ion sensor functionalized based on Fe_3O_4@SiO_2@CS magnetic ion imprinting polymer (M-IIP). The sensor is based on the coupling characteristics of the optical microfiber coupler (OMC) cone region to achieve a high sensitive response to the change of cadmium ion concentration. M-IIP materials were prepared by surface imprinting polymerization to achieve low cross-sensitivity and thus improve the detection limit of the sensor. The results show that the developed fiber sensor has high specificity and rapid response to cadmium ions. The experimental detection limit (LOD) reached 0.051 nM within 0-1 μM with a response time of less than 50 s. Moreover, the proposed fiber cadmium ion sensor has excellent performance in terms of sensitivity, stability, repeatability and biocompatibility.

1 Introduction

The high toxicity, carcinogenicity and non-biodegradation of heavy metals can damage the ecological environment and human health[1,2]. Studies show that metals with density greater than 5 kg/L are the heavy metal[3]. Cadmium is one of the most common elements of heavy metals, which has a long biological half-life[4]. Therefore, in life, long-term exposure to cadmium will lead to diseases in various human tissues, such as kidney, liver, central nervous system (CNS), and cancer in severe cases, such as kidney cancer, liver cancer and pancreatic cancer[5–7]. In drinking water, the WHO guideline value for cadmium ions was 0.003 mg/L[8].

Traditional heavy metal ion detection methods include atomic absorption spectroscopy (AAS), atomic emission spectroscopy (AES), X-ray fluorescence spectroscopy (XRF) and other[9–12]. However, these methods have some serious disadvantages. For example, although atomic absorption spectroscopy (AAS) has a high detection limit, the pretreatment requirements of the test samples are very harsh, and the anti-interference ability is relatively poor. Although atomic emission spectrometry (AES) can accurately determine the composition and concentration of elements in the sample, the operation method is complex and the types of elements are limited. Although X-ray fluorescence spectroscopy (XRF) can conduct nondestructive testing, the composition of the sample matrix is more complex, which may have a serious impact on the analysis results of XRF. Considering the above shortcomings[13,14],it is particularly important to develop a new sensor with simple operation, high sensitivity and strong anti-interference ability to meet the detection of ultra-low concentration of Cd^{2+} in aqueous solution. The advent of optical fiber sensing technology makes up for the defects of traditional detection equipment[15–17]. Recently, fiber sensing has been used in the field of cadmium ion detection[18–21]. However, these studies have varying degrees of problem. For example, [18][18] is based on the principle of surface plasmon resonance, and the need to coat the sensor surface with silver film, which significantly increases the production cost and production difficulty. The sensing unit structure of [19][19] and [20][20] leads to a limitation of the evanescent field with lower sensitivity and slower response time. [21][21] mainly rely on the surface functional group adsorption sites for cadmium ion selection. Compared with the ionic printing materials proposed in this paper, it is relatively vulnerable to other heavy metal ions, and the detection limit is insufficient. Therefore, the technologies still need to be improved in manufacturing cost, sensitivity, response time and sensor detection limits.

Ion imprinting technology uses ion as the template. After the interaction through electrostatic and coordination interaction, the holes obtained by removing the template ions are selective[22–24]

[a]Heilongjiang Province Key Laboratory of Laser Spectroscopy Technology and Application, Harbin University of Science and Technology, Harbin 150080, China
[b]Key Laboratory of Engineering Dielectrics and Its Application, Ministry of Education, Harbin University of Science and Technology, Harbin, 150080, China.
[c]School of Engineering University of Kent Canterbury, Unite K ingdom, Unite Kingdom.
* Corresponding Author Email: yuefengchn@126.com

for the target ions. Ionic imprinting is mainly composed of functional monomers and carriers, and the common functional monomers are chitosan, methacrylic acid, vinyl pyridine and vinyl imidazole. Among them, chitosan has good biocompatibility and rich surface functional groups (amino and hydroxyl groups), which has a strong chelating effect on heavy metal ions[25–27]. And the carrier includes organic carrier, inorganic carrier and biopolymer carrier. Silica dioxide (SiO_2) and ferrosoferric oxide (Fe_3O_4) used in this study are the most common inorganic carriers. SiO_2 It has the advantages of unique morphological structure, large specific surface area, high chemical stability, good mechanical properties and low preparation cost[28,29]. Fe_3O_4 has high coercive force, superparamagnetism, magnetic guide, and good biocompatibility[30,31]. Therefore, the combination of magnetic carrier and silicon-based carrier can have the characteristics of two types of materials at the same time, namely, high adsorption capacity, good thermal stability and mechanical stability.

In conclusion, in order to realize highly sensitive and highly selective detection of cadmium ions, a fiber sensor functionalized based on Fe_3O_4@SiO_2@CS magnetic ion imprinted polymer (M-IIP). OMC with strong evanescent field, low loss and easy integration and reuse is used as the optical sensing platform; M-IIP with specific adsorption is used to identify sensitive materials. The high sensitivity and high selectivity detection of Cd^{2+} in aqueous solution were achieved. When Cd^{2+} binds to the three-dimensional hole on the surface of M-IIP substrate, it will change the refractive index (RI) of M-IIP to modulate the interference spectrum. In addition, the performance of the sensor, repeatability, concentration stability and temperature sensitivity are studied in detail, and the results are discussed.

2 Sensing principle

As shown in Fig.1, is a schematic structure of the OMC used to perform cadmium ion concentration measurements. It includes a strong coupling region, two weak coupling regions. According to the coupling theory[32], when the input light with the total power of P enters from the port P1, the output power of the output port P3 and P4 is[33]:

$$P_3 = P_1 \cos^2(KL)$$
$$P_4 = P_1 \sin^2(KL) \quad (1)$$

In Equation (1), K is the coupling coefficient and L is the coupling length. However, due to the large geometric size difference, the phase difference produced by the transition region is much smaller than that produced in the uniform waist region. Therefore, the contribution of the transition zone can be ignored. Under the strong coupling condition, the coupling coefficient can be expressed as[34]:

$$K(\lambda, n_2, n_3, z) = \frac{3\pi\lambda}{32 n_2 r^2} \times \frac{1}{(1+1/V)^2} \quad (2)$$

Above(2), whereλ is the wavelength of incident light, r is the radius of the coupling zone, $V = [(2\pi r)/\lambda]\left(n_2^2 n_3^2\right)^{1/2}$ is the normalized frequency, n_2 is the refractive index (RI) of the fiber cladding, and n_3 is the RI of M-IIP.

Typically, the relationship between wavelength and cadmium ion concentration can be described by $d\lambda/dC$, which quantifies the wavelength shift caused by small changes in the concentration of cadmium ions. Therefore, the sensitivity of the OMC can be expressed as:

$$S_C = \frac{d\lambda}{dC} = \frac{\partial\lambda}{\partial n_3} \cdot \frac{dn_3}{dC} \quad (3)$$

From Eq. (3), n_2 as the refractive index of the cladding of the OMC does not vary with the cadmium ion concentration. And n_3 as the refractive index of M-IIP, i.e., the refractive index of the surrounding medium of the OMC, will change as the cadmium ions in solution bind to the three-dimensional pores on the surface of M-IIP. Since the OMC has a super strong evanescent field, and the stronger the evanescent field the stronger the ability to interact with the external environment. Under the interaction of the evanescent field, the change of n_3 affects the coupled mode transmission of the OMC, i.e., the change of the phase difference, which in turn leads to the shift of the interference spectrum of the OMC. Therefore, low concentration detection of cadmium ions can be achieved by monitoring the characteristic wavelength shift in OMC interference spectrum.

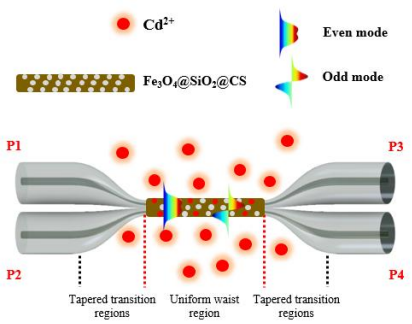

Fig. 1 Schematic diagram of the OMC sensing unit structure and transmission principle.

3 Preparation of the materials and the sensors

3.1 Source of materials required

The standard single-mode fiber used (8.2/125 μm) was purchased from Corning. The used ethylenediaminetetraacetic acid (EDTA, industrial grade 99%), was purchased from Suzhou Rentian Chemical Co., LTD. The γ-glycidyl ether oxypropyl trimethoxysilane (GPTMS) used was purchased from Shandong Qiyue Chemical Technology Co., LTD. The ethyl-silicate (silane coupling agent, TEOS) used was purchased from Jinan Hongteng Weiye New Material Co., LTD. Chitosan (99.5%) used was purchased from Qingdao Hehai Biotechnology Co., LTD. All reagents, such as cadmium chloride ($CdCl_2$), zinc chloride ($ZnCl_2$), copper chloride ($CuCl_2$), ferric chloride ($FeCl_3$), lead nitrate ($Pb(NO_3)_2$), silver nitrate ($AgNO_3$), and cobalt chloride ($CoCl_2$) were of analytical purity without further purification.

3.2 Preparation of the M-IIP material

As shown in in Fig.S1 (a), 0.4 mg of magnetic $Fe_3O_4$was added to 100 mL of 0.1 mol/L of HCl solution and dispersed by sonication for 10 min. The magnetic Fe_3O_4 was separated under an exter-

nal magnetic field, washed with distilled water, redispersed in 50 mL of ethanol, and sonicated in an ice water bath for 10 min. Then, 1 mL of ethyl silica (TEOS) and 2.4 mL of concentrated ammonia were added successively, and the ultrasonic oscillation reaction under the ice water bath was 120 min, and the products were separated under the action of the external magnetic field[35]. Take 1.14 g of cadmium nitrate and 0.25 g of chitosan in 50 mL of aqueous acetic acid solution (2% volume fraction) and stir at room temperature for 2 h. Then, 0.5 mL EGDMA was added and the reaction was stirred for 4 h at room temperature, 0.4 g Fe_3O_4@SiO_2 was added to the solution, sonicated and dispersed for 1 h, and the reaction was stirred at high speed at 60°C for 6 h. The products were separated under the external magnetic field, washed repeatedly with distilled water, and dried under vacuum at 75°C for 5 h. Subsequently, the samples were eluted with Cd^{2+} in a flask using 2g/L of ethylenediaminetetraacetic acid (EDTA) at a temperature of 30°C for 3 h. The samples obtained were washed several times with deionized water and ethanol, and then the samples were rinsed to pH neutrality with sodium hydroxide solution. Finally, M-IIP was obtained after drying with 70°C in a vacuum oven. The non-ion imprinted polymer (NIIP) was prepared in a similar way to the above preparation steps, except that cadmium ions were not added.

Fig.S1 (b) shows the infrared spectra of Fe_3O_4@SiO_2 and M-IIP. From the figure, we can find that the characteristic absorption peaks of Si-O and Fe-O are observed at around 1087 cm-1 and 570 cm-1, which not only proves the existence of SiO_2, but also indicates that SiO_2 is effectively coated on the Fe_3O_4 surface. Further for M-IIP, the wide peak appears at 3416 cm^{-1} due to the addition of CS, which overlaps the expansion vibration absorption peak of O-H and N-H. The area of the surrounding peaks increases here, mainly because the O-H and N-H expansion vibrations of chitosan increase the absorption in this range. Near 3013 cm^{-1} is the expansion vibration absorption peak of saturated C-H. At 1630 cm^{-1} is the bending vibration absorption peak of N-H. In conclusion, it indicates that CS crosslinks with Fe_3O_4@SiO_2 and the preparation of M-IIP was successfully confirmed. As shown in in Fig.S1 (c), (d) and (e), the SEM images of N-IIP, M-IIP (addition of cadmium ions) and M-IIP (removal of cadmium ions), respectively. It can be seen that N-IIP presents a uniform spherical shape. After adsorption of cadmium ions, fine particles appeared on the surface. After several washes with EDTA, deionized water and ethanol, the cadmium ions adsorbed on the surface of M-IIP were removed and the surface became rough. Further, the washed M-IIP was subjected to EDS characterization, as shown in in Fig.S1 (f), containing only iron, oxygen, silicon and carbon. The results showed that cadmium ions were cleaned. This further confirmed the successful preparation of M-IIP.

3.3 Sensor preparation

As shown in Fig.S2 is the preparation step of OMC, which is prepared by the platform shown in Fig.S2(a). The hydrogen and oxygen flame melting drawing machine pulls the two SMFs, and the spectral changes during the pulling process are monitored through the spectrometer. As shown in Fig.S2(b), the two SMFs will slowly couple into a new waveguide during the pulling process. The prepared OMC is encapsulated and then fixed on a glass sheet to enhance the mechanics and stability of the sensor.

As shown in Fig.S3, the interference spectrum for sensing is explored. As shown in Fig.S3(a), it is the interference spectrum at the diameter of different strong coupling regions. It can be found that as the diameter of the effective coupling region tatens, the length of the effective coupling region increases further, and the FSR gradually decreases[36]. When D=8.2 μm, the two waveguides are in the initial stage of mutual coupling. At D=5.8 μm, as the diameter of the effective coupling zone becomes thinner, the length of the effective coupling zone gradually increases, and the total energy begins to be able to completely couple it alternately in the two waveguide structures. As shown in Fig.S3 (c), the coupling effect of the effective coupling area becomes more and more obvious, and the energy conversion period gradually increases, which also causes additional losses, resulting in the normalized total energy value gradually decreases, and then enhances the strength of the evanescent field around the effective coupling area. As the coupling diameter becomes further finer, when the diameter is less than 3.5 μm, the interference spectrum becomes very dense at this point. The test signal of this spectrum in solution is difficult to demodulate, and it is easy to appear spectral stacking. As shown inFig.S3 (d), when the two waveguides are stretched into one waveguide, only the base mode transmission is supported in the optical fiber waveguide, and no other modes exist in the waveguide, and the interference spectrum almost disappears. This is because the conical transition region is stable, the two fibers in the effective coupling region almost melt into one, continue heating, the melting state is unchanged, and the coupling coefficient is stable. Considering the mechanical strength and convenience of the sensor, OMC with D=5.8 μm and L=3mm (as shown in Fig.S2(c)) was selected as the sensing unit for subsequent detection of Cd^{2+}, and the material surface was functionalized. Three sensing units of the same size were prepared as shown in Fig. S3(b). The results show that the FSR and extinction ratio of the interference spectra of the sensing units have the same overall trend and good repeatability. Meanwhile, the three sensors were tested for cadmium ion concentration. The results showed that the sensitivity values of the three sensors were similar. Therefore the preparation method can realize the repeatable preparation of the sensing unit.

Fig.S4 shows the sensitive material functionalization modification step in OMC. The prepared OMC was first soaked to a standard NaOH solution for 30 min, then rinsed 3-5 times with deionized water and then dried completely. Next, the fibers were placed in APTES solution (ethanol:deionized water (9:1 v/v); concentration 2%) for 1 hour. This process is silanization of the fiber. The fibers were then thoroughly rinsed 3-4 times with the ethanol solution and placed in an oven at 60°C for 2 hours. Finally, the modified OMC was immersed in the prepared M-IIP sensitive material solution for 30 min, until the material was fully combined to the fiber surface. This was then rinsed thoroughly with deionized (DI) water and left in a 75°C oven for 4 hours.

In the preparation process of modifying sensitive materials on fiber surface, different concentrations of sensitive materials will

lead to different effects of modification on the surface of fiber fiber, and then affect the output effect of sensor interference spectrum. Therefore, three different concentrations of M-IIP sensitive materials, 0.1 Mol/L, 0.5 Mol/L and 1 Mol/L, were prepared to modify the effective coupling region of OMC with a modification time of 30 min. As shown in Fig.S5, which is the interference spectral changes of OMC before and after modification of M-IIP sensitive materials. It can be found that the interference spectrum of modified sensitive materials has different degrees of displacement phenomenon and weakened extinction ratio phenomenon. This is due to the sensitive material modification in the coupling region of OMC, and the effective refractive index of the two supermodes of OMC is modulated by the refractive index coefficient of the sensitive material itself, resulting in different degrees of displacement of the interference spectra. However, different concentrations of sensitive materials will affect the extinction ratio of the interference spectrum. The higher the concentration of sensitive materials, the more serious the light absorption, the greater the transmission loss, and the smaller the extinction. Combined with the above discussion, the higher the extinction ratio, the easier the sensor is for demodulation. Therefore, an OMC sensor modified with 0.1 Mol/L of M-IIP was selected for the detection of Cd^{2+}.

4 Sensor performance analysis and cadmium ion detection

4.1 Figures

As shown in Fig. 2, the detection device mainly includes amplified spontaneous emission light source (ASE) (1500 nm 1620 nm, Kangguan, China), polarization controller, sensing unit OMC and optical spectrum analyzer (OSA, AQ6370D, Yokogawa, Japan). First, different concentrations of Cd^{2+} (0-1 μM) solutions were prepared by a diluted 1 Mol/L of $CdCl_2$ solution. The spectral response of OMC to the Cd^{2+} solution was recorded at room temperature (T=25°C). Note that, after each test concentration, the cone region of the OMC was washed with EDTA diluted in deionized water until the spectrum was stabilized before the next concentration test.

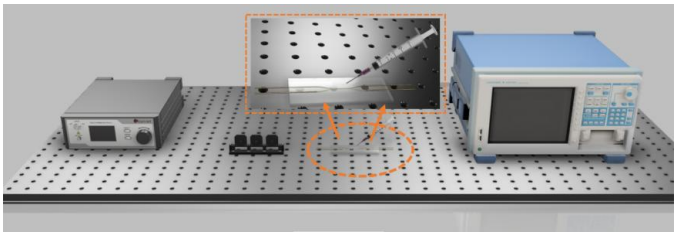

Fig. 2 Cd^{2+} detection experimental setup Fig.

As shown in Fig. 3(a) and 3 (b), the redshift of the disturbed valley occurs with the increase of Cd^{2+} concentration in the concentration range of 0-1 μM. As shown in Fig.3(a), the maximum sensitivity of the OMC without cladding sensitive material was 1087.16 nm/μM with a linear fit of about 0.995. As shown in Fig.3(c), an OMC with NIIP has a maximum sensitivity of up to 3611.33 nm/μM and a linear fit of about 0.95. As shown in

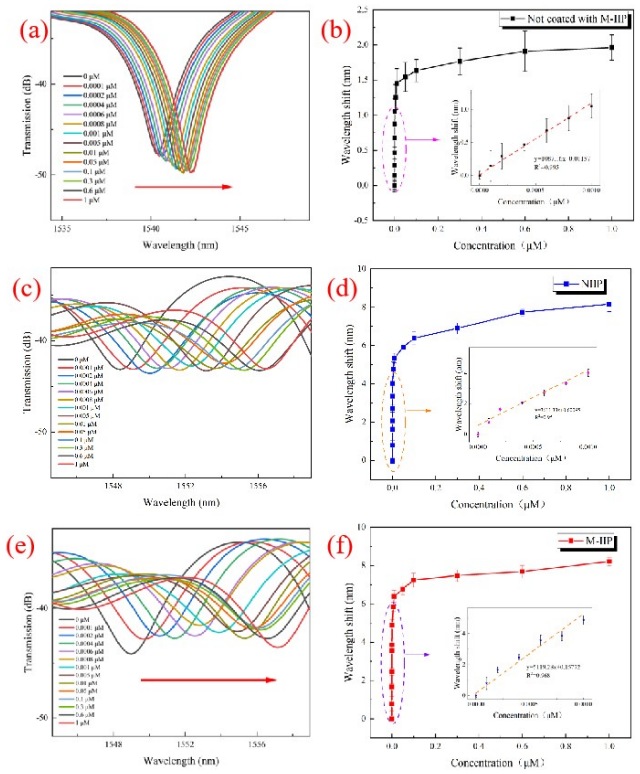

Fig. 3 (a) OMC interference spectra of unmodified sensitive materials; (b) sensitivity fitting of unmodified sensitive materials; (c) OMC interference spectra of modified NIIP; (d) sensitivity fitting of NIIP/OMC; (e) OMC interference spectra of modified M-IIP; (f) sensitivity fitting of M-IIP/OMC.

Fig.3(e), an OMC with modified M-IIP has a maximum sensitivity of up to 5119.28 nm/μM and a linear fit of about 0.968. By comparison, it can be seen that the M-IIP/OMC has the highest sensitivity when tested in the low concentration region. It showed a 4.7-fold increase in sensitivity over the sensor without the sensitive material encapsulated. It is 1.4 times more sensitive than NIIP/OMC, and has an ultra-low concentration detection limit of 0.051 nM(LOD=3σ/k, σ Is the standard deviation of the blank signal, and k is the slope of the linear calibration plot). This is due to the adsorption of Cd^{2+} by the three-dimensional holes on the M-IIP surface and the strong chelation of the surface functional groups-OH and-NH_2. Therefore, the sensor modifying M-IIP has obvious effect and high sensitivity. With the increasing concentration of Cd^{2+}, increasing amounts of Cd^{2+} are complexed with the three-dimensional holes and surface functional group binding sites on the M-IIP surface, changing the refractive index of sensitive materials. It also causes the effective RI enlargement between the two supermodes of the OMC, which then leads to the interfering spectral redshift. However, with the further increase of Cd^{2+} concentration, the binding site on the surface of sensitive materials becomes saturated, and the upper limit of the sensor is reached. Therefore, the sensitivity of the sensor was significantly reduced in the concentration range of 0.001-1 μM. The sensor modifying M-IIP is effective, so a series of sensor performance tests will be tested in subsequent tests.

Response time test: As shown in Fig.4, it is the response time

test of the sensor. The response time of sensors at 0.0001 μM, 0.001 μM and 0.01 μM (pH = 6 to 7). The results show that the response times of this sensor at different Cd^{2+} concentrations were approximately 34s (0.0001 μM), 21s (0.001 μM), and 13s (0.01 μM), respectively. It can be found that the larger the Cd^{2+} concentration, the faster the response time of the sensor reaches a saturation wavelength shift of 90%, because the larger the Cd^{2+}concentration, the higher the rate of its binding to the surface binding site of sensitive materials.

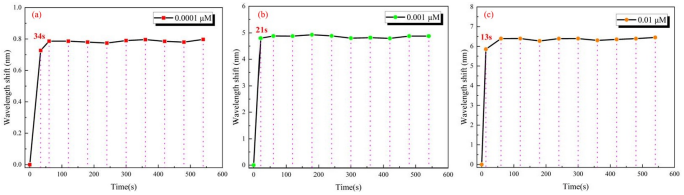

Fig. 4 Response time of the sensor at different concentrations: (a) C=0.0001 μM; (b) C=0.001 μM; (c) C=0.01 μM.

As shown in Fig.5(a), the stability of the sensor was tested at different concentrations: 0.0001 μM 0.01 μM Cd^{2+} solutions (pH = 6-7) were dropped into the coupling area of the sensor. The results show that the sensor exhibits long-term stability after reaching the maximum wavelength shift at this concentration, with a maximum fluctuation not exceeding ± 0.5nm. The slight deviation is mainly affected by the external conditions such as the resolution of the OSA, the ambient temperature, and the intensity fluctuation of the light intensity. Repeatability testing of sensors is an important factor in evaluating sensor performance. The repeatability of the sensor at 0-1 μM was tested as shown in Fig.5(b). The sensors were first placed into different concentrations of cadmium ion solutions ranging from 0-1 μM, and the spectra were stabilized and recorded. After each test, the sensor needs to be thoroughly cleaned and dried using hydrochloric acid and sodium hydroxide solutions. It can be noticed that after thorough cleaning and drying, the spectrum can be returned to the initial reference spectral position. After five cycles of testing, the wavelength shift fluctuation of each test was small, and the fluctuation range was kept around ±0.5 nm. The OMC sensor proved to have good repeatability. As shown in Fig.5(c), the effect of the sensor on its sensing performance at the Cd^{2+}concentration of 0.001 μM (2,3,4,5,6,7,8,9,10,11). In the acidic environment(pH <7), the amino and hydroxyl groups on the surface of M-IIP are easily protonated to generate positively charged-NH^{2+}, which forms electrostatic repulsion with positively charged Cd^{2+}, resulting in a weak coordination effect; Meanwhile, the H^{+} present in solution underwent competitive adsorption to the binding site on the M-IIP surface, so that the interference spectra move less and the sensor response is weak in a more acidic environment. As the pH increases, the group is deprotonated and negatively charged, the binding site coordination effect increases, the complexation reaction with the positively charged $Cd^{2+}$to form complexes, and disturb the spectrum to reach the maximum displacement value close to pH=7. When pH> 8, tends to an alkaline environment, Cd^{2+} gradually forms a precipitate with OH^{-}, and the concentration of cadmium ions in solution decreases, thus resulting in the amount of interference spectral shift. Therefore, the best suitable condition for this sensor is around a pH of 6 to 7. The selectivity of the M-IIP/OMC sensor was tested as shown inFig.5(d). Cd^{2+}, Zn^{2+}, Ag^{+}, Cu^{2+}, Pb^{2+}, Fe^{3+}, Co^{2+}, Pb^{2+}, Na^{+}, K^{+}, Ca^{2+}, Cl^{-}, Mg^{2+} solutions with concentrations of 0.0006 μM, 0.001 μM, and 0.01 μM were tested. The results showed that the wavelength shift induced by Cd^{2+} was 6-10 times higher than that of the other 12 ions and remained selective in the mixture of the 12 ions. It shows that the sensor has good selectivity for Cd^{2+}.

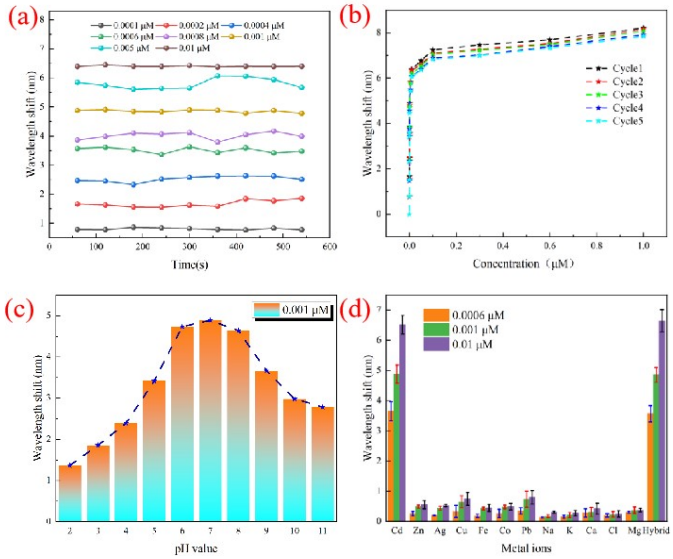

Fig. 5 (a) Stability of the sensor at different concentrations (C=0.0001 μM 0.01 μM); (b) Reproducibility test of the sensor; (c) Sensor response at the pH values of different solutions; (d) The selectivity of the sensors for the different metal ions.

Effect of temperature: As shown in Fig. 6, the temperature sensitivity of the sensor was tested in the range of 25-55°C for one step size per 5°C. The results show that the wavelength sensitivity of this sensor is 125.66 pm/°C, which is several times different than the sensor sensitivity to Cd^{2+} solution concentration. In the optimal temperature monitoring range of 25-35°C, the maximum wavelength shift is only 1.5 nm, and the wavelength shift is very small and negligible. This indicates that the sensor is less sensitive to temperature, which facilitates the detection of Cd^{2+}.

As shown in Table1, the sensing performance of several fiber optic cadmium ion sensors is compared. It can be noticed that the present study has higher sensitivity (5119.28 nm/μM) and lower detection limit (0.051nM) compared to the work done by [17-21] [17–21] . However, the sensor also has some limitations, such as the sensor relies on a high-precision spectral analyzer and a highly stable ASE light source, which is still expensive in the construction cost of the overall system. Meanwhile, the mechanical strength of the sensing unit is low, and the coating uniformity of M-IIP is not easy to control, which needs to improve the preparation process of the sensing unit in the subsequent research.

5 Conclusions

In conclusion, M-IIP sensitive materials can achieve ultra-high selectivity for Cd^{2+}. However, the proposed fiber optic cadmium ion

Table 1 Comparison of the sensing performance of different types of Cd^{2+} fiber sensors

Method	sensitive material	concentration range(μM)	maximum sensitivity (nm/μM)	LOD	advantages	inadequate	Refs
Reflection	BSA/Au	0-1	76.67	7.1 nM	Easy to carry, high mechanical strength and easy to control material thickness.	Low sensitivity, expensive material costs, and high optical signal noise.	[17] [17]
Reflection	Ag-PVA/TiO_2	0-1	315.2	6 nM	Flexible structure of the sensing unit and easy control of the material thickness.	High material cost, difficult sensor preparation process, narrow detection range and poor detection limit	[18] [18]
Transmission	α-Fe_2O_3@MoS_2	0-100	475.19	1.42 nM	Wide detection range, flexible structure of sensing unit and simple preparation process.	Low response time, material coatings are not easily controlled, and detection limits are poor.	[19] [19]
Transmission	SnO_2-MoS_2	0-100	0.03	-	The sensing unit has a flexible structure, a wide detectionrange and a simple preparation process.	Long response time, low sensitivity, material thickness is not easy to control.	[20] [20]
Reflection	propylene thiourea membrane	0-12	0.051	400 nM	Dual parametric demodulation, flexible structure of the sensing unit and easy control of the material thickness.	Low sensitivity and poor detection limits	[21] [21]
Transmission	M-IIP	0-1	5119.28	0.051 nM	High sensitivity, low detection limit, simple preparationprocess, low preparation cost and fast response time.	Poor mechanical strength, material thicknessis not easy to control, narrow detection range.	This work

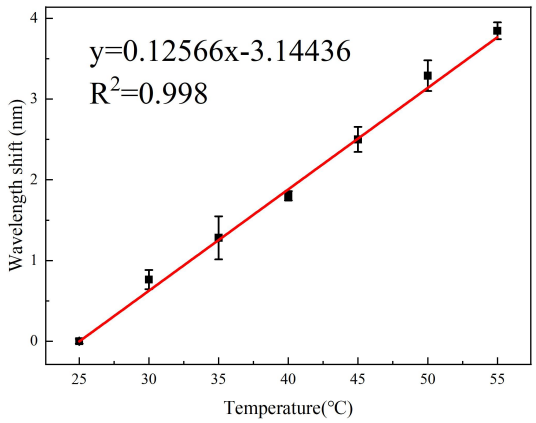

Fig. 6 Linear fitting of the spectral shift at different temperatures (25-60℃).

sensor based on M-IIP functionalization has reached a good level in the sensitivity, detection limit, response time and repeatability of Cd^{2+}, which can realize trace detection at nM level and high repetitive use. At the same time, the sensor preparation process is based on single mode fiber, the cost of the material is relatively low. Based on the above points, compared with the traditional heavy metal ion detection platform, the sensor has new potential applications in the detection of ultra-low concentration of heavy metal ions.

Data availability

Data underlying the results presented in this paper are not publicly available at this time but may be obtained from the authors upon reasonable request.

Conflicts of interest

There are no conflicts to declare.

Acknowledgements

This work was supported by National Natural Science Foundation of China(No.52102164: Construction of functionalized M_3C_2Tx MXene/graphene aerogel and its gas-sensitive properties); Heilongjiang Province Natural Science Foundation of China(No. ZD2023E006: Research on optical fiber magnetic field monitoring information fusion of Marine shipping submarine cable lines based on optical thermal tweezers compensation); Harbin manufacturing science and technology innovation talent project(No.2022CXRCCG003:Development and marketing of optical detection system for partial discharge of power transformer);Project to Enlist Young Scientific and Technological Talents in Heilongjiang Province (2022QNTJ004); "Outstanding Master's and Doctor's Degree Thesis of Longjiang in New Age" Project Support (LJYXL2022-064).

Notes and references

1 G. Genchi, M. S. Sinicropi, G. Lauria, A. Carocci and A. Catalano, *International journal of environmental research and public health*, 2020, **17**, 3782.

2 L. S. Di Toppi and R. Gabbrielli, *Environmental and experimental botany*, 1999, **41**, 105–130.

3 P. Goering, M. Waalkes and C. Klaassen, *Toxicology of metals: biochemical aspects*, Springer, 1995, pp. 189–214.

4 M. P. Waalkes, *Mutation Research/Fundamental and Molecular Mechanisms of Mutagenesis*, 2003, **533**, 107–120.

5 M. Waisberg, P. Joseph, B. Hale and D. Beyersmann, *Toxicology*, 2003, **192**, 95–117.

6 S. Satarug, S. H. Garrett, M. A. Sens and D. A. Sens, *Environmental health perspectives*, 2010, **118**, 182–190.

7 L. Järup and A. Åkesson, *Toxicology and applied pharmacology*, 2009, **238**, 201–208.

8 W. H. Organization, *Guidelines for drinking-water quality*, World Health Organization, 2004, vol. 1.

9 J. W. Robinson, *Analytical Chemistry*, 1960, **32**, 17A–29A.

10 J. D. Winefordner and R. C. Elser, *Analytical Chemistry*, 1971, **43**, 24A–42a.

11 P. J. Potts and P. C. Webb, *Journal of Geochemical Exploration*, 1992, **44**, 251–296.

12 R. Sitko and B. Zawisza, *X-ray spectroscopy*, 2012, 137–162.

13 D. Sanchez-Rodas, W. Corns, B. Chen and P. Stockwell, *Journal of Analytical Atomic Spectrometry*, 2010, **25**, 933–946.

14 S. Greenfield, *Spectrochimica Acta Part B: Atomic Spectroscopy*, 1983, **38**, 93–105.

15 T. Yang, C. Liu, X. Liu, Y. Feng, T. Shen and W. Han, *Optics Communications*, 2022, **515**, 128222.

16 X. Li, N. Wang, F. Wang, J. Liu, Y. Shi, J. Jiang, H. Liu, M. Li, L. Zhang, W. Zhang *et al.*, *Analyst*, 2023, **148**, 1672–1681.

17 B.-G. Şolomonea, L.-I. Jinga, V.-A. Antohe, G. Socol and I. Antohe, *Biosensors*, 2022, **12**, 573.

18 T. Li and W. Feng, *IEEE Sensors Journal*, 2021, **21**, 18650–18655.

19 T. Yang, W. Yuan, Y. Feng, C. Liu and T. Shen, *Sensors and Actuators A: Physical*, 2023, **355**, 114322.

20 H. Chen, X. Yang and W. Feng, *Applied Optics*, 2021, **60**, 799–804.

21 T. Yang, Y. Feng, W. Yuan, C. Liu and T. Shen, *IEEE Sensors Journal*, 2023.

22 D. Li, Z. Bie, F. Wang and E. Guo, *Analyst*, 2018, **143**, 4936–4943.

23 B. B. Yola, S. Bekerecioğlu, İ. Polat, N. Atar and M. L. Yola, *Analyst*, 2023.

24 J. Li, J. Fu, Q. Yang, L. Wang, X. Wang and L. Chen, *Analyst*, 2018, **143**, 3570–3578.

25 M. Yan, R. Wang, Y. Li, X. Kang, Z. Zhang, Y. Li and M. Jiang, *Analyst*, 2023, **148**, 1075–1084.

26 R. Gupta and N. J. Goddard, *Analyst*, 2021, **146**, 4964–4971.

27 S. Tripathy, A. K. Chalana, A. Talukdar, P. Rajesh, A. Saha, G. Pramanik and S. Ghosh, *Analyst*, 2022, **147**, 165–177.

28 W. Xue, J. Zhong, H. Wu, J. Zhang and Y. Chi, *Analyst*, 2021, **146**, 7545–7553.

29 D. G. Schlom, S. Guha and S. Datta, *MRS bulletin*, 2008, **33**, 1017–1025.

30 X. Deng, W. Li, G. Ding and X. Chen, *Analyst*, 2018, **143**, 2665–2673.

31 J. Sun, S. Zhou, P. Hou, Y. Yang, J. Weng, X. Li and M. Li, *Journal of biomedical materials research Part A*, 2007, **80**, 333–341.

32 J. Wen, X. Yan, X. Gao, K. Li and J. Wang, *IEEE Sensors Journal*, 2022, **22**, 4090–4095.

33 K. Li, N. M. Y. Zhang, N. Zhang, T. Zhang, G. Liu and L. Wei, *Journal of Lightwave Technology*, 2018, **36**, 2409–2415.

34 K. Li, N. Zhang, N. M. Y. Zhang, G. Liu, T. Zhang and L. Wei, *Optics letters*, 2018, **43**, 679–682.

35 F. Ding, Y. Zhao, H. Liu and W. Zhang, *Analyst*, 2020, **145**, 4341–4351.

36 M. Yuan, S. Pu, D. Li, Y. Li, Z. Hao, Y. Zhang, C. Zhang and S. Yan, *Results in Physics*, 2021, **29**, 104743.